Computers & Graphics 124 (2024) 104070

Contents lists available at ScienceDirect

Computers & Graphics

journal homepage: www.elsevier.com/locate/cag

Special Section on EG VCBM 2024

# Synthetic surface mesh generation of aortic dissections using statistical shape modeling

Kai Ostendorf [a,*], Kathrin Bäumler [b], Domenico Mastrodicasa [c], Dominik Fleischmann [b], Bernhard Preim [a], Gabriel Mistelbauer [b]

[a] Dept. of Simulation & Graphics, Otto-von-Guericke University Magdeburg, Germany
[b] Dept. of Radiology, Stanford University School of Medicine, USA
[c] Dept. of Radiology, Washington University School of Medicine, USA

ARTICLE INFO

*Keywords:*
Object modeling
Statistical shape modeling
Synthetic cohort generation
Aortic dissection

ABSTRACT

Aortic dissection is a rare disease affecting the aortic wall layers splitting the aortic lumen into two flow channels: the true and false lumen. The rarity of the disease leads to a sparsity of available datasets resulting in a low amount of available training data for in-silico studies or the training of machine learning algorithms. To mitigate this issue, we use statistical shape modeling to create a database of Stanford type B dissection surface meshes. We account for the complex disease anatomy by modeling two separate flow channels in the aorta, the true and false lumen. Former approaches mainly modeled the aortic arch including its branches but not two separate flow channels inside the aorta. To our knowledge, our approach is the first to attempt generating synthetic aortic dissection surface meshes. For the statistical shape model, the aorta is parameterized using the centerlines of the respective lumen and the according ellipses describing the cross-section of the lumen while being aligned along the centerline employing rotation-minimizing frames. To evaluate our approach we introduce disease-specific quality criteria by investigating the torsion and twist of the true lumen.

## 1. Introduction

Aortic dissection is a life-threatening disease [1], characterized by the separation of the aortic media layer due to a tear in the aortic intima. Since blood is able to enter the media, it gradually forms a new flow channel (false lumen) besides the existing true lumen. Both these lumina are separated by the intimo-medial flap, referred to as dissection flap. The weakened outer wall of the false lumen is prone to dilation over time, which can lead to serious complications such as aortic rupture and pericardial tamponade. To identify and prevent these complications, patients require life-long monitoring via imaging.

Advanced imaging techniques enable the extraction of aortic surface meshes for non-invasive assessment of anatomical and hemodynamic features. Since aortic dissection is a rather rare disease, it is difficult to obtain comprehensive datasets. To overcome this limited availability and obtain a more holistic view of the disease, synthetic data have proven to be a promising alternative. The generation of synthetic datasets can compensate for the lack of real data and improve the development of artificial intelligence-based models for predicting and analyzing patients with aortic dissection. The approach presented in this paper can therefore improve machine learning (ML) applications in the field of aortic dissection by increasing the availability of imaging data.

Machine learning (ML) models have been used to create synthetic surface geometry of healthy blood vessels [2,3]. Synthetic databases of aortic surface meshes were created for the aortic arch [4] and the thoracic aorta including its branches [5]. Synthetic cohorts were generated to investigate the diseased aorta regarding thoracic aortic aneurysm [6] and coarctation of the aorta [7]. However, the investigation of aortic dissection generation remains rather unexplored. This is further complicated by the multiple, possibly intertwined, flow channels. There are currently no large databases of synthetic 3D surface meshes of aortic dissections that could be used by researchers to develop and test new approaches. Furthermore, existing approaches focus on the generation of aortic or other vessel geometry containing only a single flow channel.

In this work, we present an automated workflow to generate synthetic surface meshes of aortic dissections. This includes modeling the aorta with two lumina (true and false). To assess the quality of the generated surface meshes, we use data- and clinically-driven quality criteria. The effectiveness of these criteria is then evaluated by medical experts. To further substantiate the plausibility of the generated surface meshes, we present CFD simulation results. Our contributions are:

* Corresponding author.
*E-mail address:* kai.ostendorf@ovgu.de (K. Ostendorf).

https://doi.org/10.1016/j.cag.2024.104070
Received 3 May 2024; Received in revised form 27 August 2024; Accepted 3 September 2024
Available online 6 September 2024

**Table 1**
Comparison of prior works.

| Papers/Criteria | Motivation | Method | # Datasets | # Lumina | Region | Representation |
|---|---|---|---|---|---|---|
| Danu et al. [2] | Support development of data-driven models. | VAE, GAN | 10000 (with augmentation) | 1 | • Segments of vessel-like structures<br>• Segments of coronary arteries | Voxel-based |
| Thamsen et al. [7] | Support ML approaches with large training database. | SSM | 154 | 1 | • Ascending aorta<br>• Aortic arch (incl. 3 branches)<br>• Descending aorta | Centerline and radii defining circular cross-sections of aorta and branches |
| Romero et al. [9] | Support in-silico analysis with 3D image dataset availability of rare cases. | SSM | 26 | 1 | • Entire aorta without branches | Centerline as cubic B-spline and additional spline for each centerline point describing wall |
| Wiputra et al. [5] | Mitigate the lack of large datasets that could be used for the fitting, training, and testing of a correlative model. | SSM | 33 | 1 | • Aortic root to distal end of the model | Centerline and cylindrical coordinate system described by vessel radius and polar angle. |
| Beetz et al. [10] | Correctly represent inter-person differences and enable more personalized and accurate computer models. | VAE | 1300 | – | • Heart | Point cloud |
| Feldman et al. [3] | Accurate 3D models of blood vessels are increasingly required for several purposes in medicine and science. | VAE | 1694 | 1 | • Blood vessel segments | Centerline and radii |
| **Our contribution** | First step towards steerable datasets of aortic dissection for CFD simulations and ML approaches. | SSM | 100 | 2 | • Aortic root to aortic bifurcation | Separate centerlines for the aorta and true lumen, walls approximated by ellipses |

- a method to create synthetic Stanford type B aortic dissection [8] surface meshes using SSM containing two flow channels,
- disease-specific quality criteria, such as torsion, diameter, and area ratios between the lumina,
- automatic rejection of unphysiological synthetic shapes and quality assessment based on these criteria.

To our knowledge, the inclusion of a second flow channel in the generation of an aortic (or any other vessel) geometry has not yet been investigated. The most relevant prior contributions are compared in Table 1.

## 2. Related work

In the following section, we aim to give a detailed overview of the past and current approaches regarding the generation of virtual patient cohorts using statistical shape modeling and machine learning approaches that focus especially on the generation of aortic geometries or other related geometries to underline our contribution.

### 2.1. Cohort generation using statistical shape modeling

Statistical shape modeling [11] is widely used to generate various anatomical geometries for different tasks, such as image segmentation [12] and image analysis. In recent years SSM were employed to generate synthetic patient cohorts for in-silico trials [13,14] or to train ML models [7,9].

Catalano et al. [6] developed a SSM of ascending thoracic aortic aneurysm to evaluate its hemodynamics. They used a cohort of 106 patients equally split into two groups with bicuspid aortic valve and normal tricuspid aortic valve. The 3D surface models included the aortic valve, the ascending aorta, the aortic arch (excluding branching vessels) and the descending aorta. By performing CFD simulations on the generated geometry the authors could link shape modes like aneurysm size and tortuosity to various flow parameters.

Romero et al. [9] assessed different strategies to increase the sampling efficiency and control statistical properties of synthetic cohorts of the thoracic aorta. The aortic geometry of 26 cases was represented using a cubic B-spline curve of the centerline with the respective radii following the approach of Romero et al. [15]. A SSM was built by performing a PCA on the input population. Three sampling strategies were examined including non-parametric sampling using bootstrapping, parametric sampling using a multivariate Gaussian distribution and a uniform distribution, and a generative adversarial network (GAN). In total 3000 synthetic shapes were created. The sampling strategies were evaluated using data-driven, clinically-driven, and feature space-driven acceptance criteria.

Thamsen et al. [7] generated a database of 2652 virtual cases containing aortic morphometry and hemodynamics using statistical shape modeling to capture the 3D shape variability of patients with coarctation of the aorta. They used a centerline-based shape description of the aorta containing the centerline coordinates including the three side branches of the aortic arch and respective radii. Additionally, two SSMs of velocity inlet profiles were created one for patients with tricuspid aortic valves and one for patients with bicuspid aortic valve defect. Using the three SSMs, a database of more than 10000 synthetic cases was created by randomizing the weights of the modes of shape variation using a normal distribution. Next, a stepwise filtering approach was employed to remove unphysiological shapes from the database. The shapes were filtered according to their radii and branches intersecting with the aortic arch. CFD simulations were performed on the remaining cases generating a cohort of synthetic models containing morphology and hemodynamic information. 2537 of these models were then used to develop a peak systolic pressure gradient prediction model for the coarctation of the aorta that could outperform the current Bernoulli-based approach.

Wiputra et al. [5] created a SSM of the thoracic aorta including the three major branches of the aortic arch. The model included input data from 33 patients and parameterized the aorta and branches using

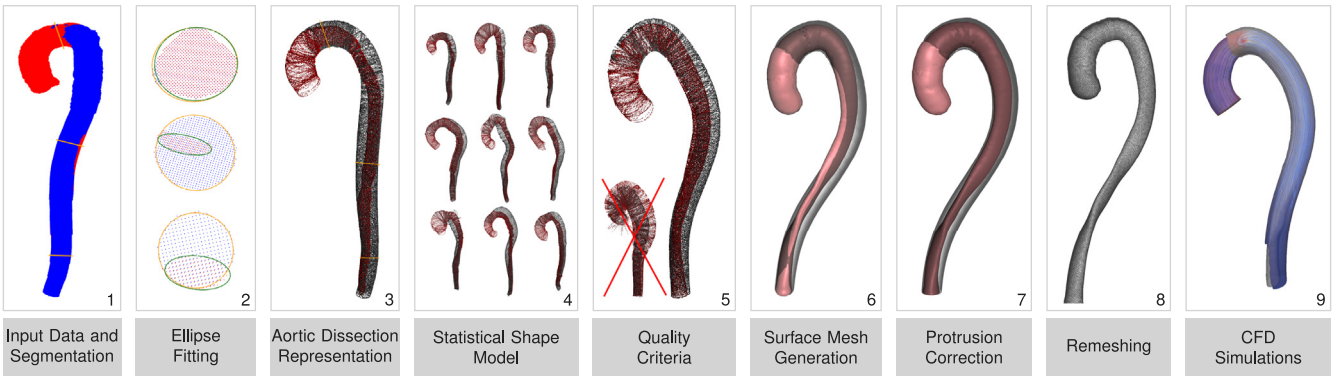


**Fig. 1.** Workflow to generate synthetic aortic dissection surface meshes. Starting from the left with the input data in the form of segmentation masks for the true and false lumen (1) ellipses are fitted to the aortic wall and the true lumen (2) to create the ellipse-based representation (3). From the representations of the input data, an SSM is built (4). Multiplying the PCs with random weights inside the ranges of $[-\lambda, \lambda]$ synthetic shapes are generated and filtered based on our clinically- and data-driven quality criteria (5). If a shape is accepted surface meshes are generated for the aorta and the true lumen (6). Next, possible protrusions of the true lumen are fixed using boolean mesh operations truncating the true lumen (7). Afterward, the surface meshes are remeshed to create mostly equilateral triangles with angles greater than 45°(8). Lastly, some manual steps have to be performed to run CFD simulations on the surface meshes (9). Up until the last step (9), this workflow is completely automated.

centerlines combined with a cylindrical coordinate system including the vessel radius and polar angles. CFD simulations were performed on two of the generated geometries to investigate how the flow profiles were affected by the representation.

Bridio et al. [13] generated a virtual cohort of patients of acute ischemic stroke treatments to support in-silico trials. SSM was used to create 83 models of cerebrovascular anatomies based on 88 patient datasets. The vessel geometries were parameterized using their corresponding centerlines and diameters. The acceptance criterion for virtual patients was based on evaluating bends for their average diameter, curvature values and tortuosity as well as angles at bifurcations.

Verstraeten et al. [14] developed a virtual cohort generator capable of automatically generating synthetic aortic valve stenosis geometries to populate a virtual patient cohort for in-silico trials. The generator employs the SSM framework of Durrleman et al. [16] generating geometries based on data- and clinically-driven acceptance criteria based on input data of 97 patients.

### 2.2. Cohort generation using machine learning approaches

The generative power of ML models has been of great interest in recent years. The generation of synthetic anatomical surface meshes using these models is still a smaller field of research but progress is being made using various architectures like variational auto encoders (VAEs) and GANs to create vessel-like structures [2,3] or the anatomy of the heart [10].

Danu et al. [2] generate synthetic blood vessel surfaces using GAN and VAE approaches. Input data in the form of surface meshes is voxelized to a size of $128 \times 32 \times 32$. Their models generate 2D images of vessel-like structures, 3D voxelizations of vessel-like structures, and 3D voxelizations of real anatomical models reconstructed from medical images.

Beetz et al. [10] proposed a multi-domain VAE, combining the modeling of biventricular anatomy and cardiac electrophysiology. As training data, magnetic resonance images and electrocardiograms (ECG) were acquired from 1300 subjects of the United Kingdom Biobank imaging study [17]. Point clouds at the end of systole (ES) and the end of diastole (ED) were computed from the imaging data and, together with the ECGs, used as input for the VAE. The proposed VAE can generate realistic ECGs, ES point clouds, and ED point clouds when randomly sampling from the latent space distribution. Feldman et al. [3] presented VesselVAE a Variational Autoencoder to create synthetic 3D surface meshes of blood vessels. The network takes as input a binary tree representation of the blood vessel 3D geometry, which is then processed using a Recursive variational Neural Network consisting of an encoder and a decoder. Subsequently, the method of Felkel et al. [18] is used to generate a surface mesh from the reconstructed tree which is smoothed and has its resolution increased using the Catmull–Clark subdivision algorithm [19]. To evaluate their approach they, analyzed the tortuosity per branch, the vessel centerline total length, the average radius of the tree, and the cosine similarity.

In line with recent approaches, our goal is to create a cohort of synthetic aortic dissection surface meshes modeling a second flow channel representing the true lumen inside the aorta.

## 3. Methodology

The goal of this work is to generate realistic synthetic surface meshes of aortic dissections. To this end, we model the aorta and the true lumen using their centerlines with an elliptical cross-section. The false lumen is implicitly modeled as the subtraction of the true lumen from the aorta (Section 4.3). Unphysiological shapes are then filtered using data- and clinically-driven criteria. The entire workflow is shown in Fig. 1 and each step is subsequently explained.

### 3.1. Input data and segmentation

Our workflow starts with the segmentation masks of the true and false lumen as input, including the centerline of the aorta and the computed tomography angiography (CTA) dataset. Additionally, we reformatted the data and masks along this centerline, in the so-called multiplanar reformation (MPR) space with an equidistant sampling interval of 1 mm for all our datasets.

### 3.2. Ellipse fitting

As we focus on elliptical cross-section in this work, we fit ellipses to the entire aorta (true and false lumen) and the true lumen in MPR space. The center point of each ellipse is then used to update the centerlines of the aorta and true lumen, respectively. The ellipse fitting is performed by singular value decomposition (SVD) on the corresponding aortic and true lumen pixels in each MPR slice. This results in eigenvectors representing the major and minor axes of the aorta $(a_a, b_a)$ and true lumen ellipse $(a_{tl}, b_{tl})$, with the eigenvalues representing the axes lengths $(|a_a|, |b_a|, |a_{tl}|, |b_{tl}|)$. The ellipse fitting can capture the area of the aorta and true lumen to an accuracy of 5% (Fig. 6).

**Table 2**
Value ranges presented in our datasets. $(a_a, b_a)$ and $(a_{tl}, b_{tl})$ are the major and minor axes of the aorta and true lumen ellipses, respectively.

| Property | Values in mm | | |
|---|---|---|---|
| Aorta centerline length (min, max, avg) | 436 | 7090 | 5660 |
| Aorta radii $a_a$ (1st qt, avg, 3rd qt) | 13.9 | 17.1 | 28.5 |
| Aorta radii $b_a$ (1st qt, avg, 3rd qt) | 13.9 | 17.2 | 26.4 |
| True lumen radii $a_{tl}$ (1st qt, avg, 3rd qt) | 13.1 | 16.4 | 20.3 |
| True lumen radii $b_{tl}$ (1st qt, avg, 3rd qt) | 13.3 | 16.7 | 20.6 |
| False lumen starts (min, avg, max) | 0 | 192 | 312 |
| Largest radii change aorta ($a_a$, $b_a$) | 6 | 1.6 | |
| Largest radii change true lumen ($a_{tl}$, $b_{tl}$) | 6 | 3.8 | |

### 3.3. Aortic dissection representation

Next, we fit cubic b-splines $x(u)$ through the centerline points to compute the aortic and true lumen centerlines in physical coordinate space, respectively. For every centerline point, we calculate the tangent $t(u)$ of the curve. The tangents are used to calculate the rotation-minimizing frame (RMF) following the approach of Wang et al. [20]. For each centerline point a local reference frame is created consisting of $t(u)$, and two orthonormal vectors $s(u)$ and $r(u)$ lying in the plane of the aorta and true lumen wall points. Starting from the aortic root and continuing to the aortic bifurcation, these frames are aligned along the aorta to minimize their rotation. The frames define the transformation between physical coordinate space and MPR space. Motivated by prior work in vessel visualization and modeling [21,22], we employ RMFs instead of the commonly used Frenet-Frame [15,23,24]. This avoids sudden changes of direction that could introduce errors when determining the ellipse angles, as discussed next. Since the major axis of an ellipse can point towards two directions flipped by 180°, we choose the major axis direction in the following way. Starting from the aortic root, we choose the major axis direction forming the smallest angle between the major axis and $s(t)$. In the subsequent slices, we choose the major axis direction that forms the smallest angle between this slice's major axis direction and the previous slice's major axis direction. This is repeated until all slices are processed.

To establish correspondences between the orientations of the ellipses across different datasets, the local reference frame is used to calculate the angle $\phi_a$ between the major axis of the aorta $a_a$ and $s(t)$. The true lumen angle $\phi_{tl}$ is calculated using the major axis $a_{tl}$ of the true lumen ellipse and $s(t)$.

With the centerlines and ellipses calculated for the aorta and true lumen, a single slice can be represented using the location of the corresponding centerline point of the aorta $(x_a, y_a, z_a)$ and the true lumen $(x_{tl}, y_{tl}, z_{tl})$, the length of the major and minor axes $|a_a|, |b_a|, |a_{tl}|, |b_{tl}|$, and their respective angles $\phi_a$ and $\phi_{tl}$. Combining this slice representation for the entire aorta, we can represent a single aortic dissection dataset $\mathbf{D}$ as:

$$\mathbf{D} = \begin{bmatrix} (x_a, y_a, z_a, |a_a|, |b_a|, \phi_a, x_{tl}, y_{tl}, z_{tl}, |a_{tl}|, |b_{tl}|, \phi_{tl})_0 \\ \vdots \\ (x_a, y_a, z_a, |a_a|, |b_a|, \phi_a, x_{tl}, y_{tl}, z_{tl}, |a_{tl}|, |b_{tl}|, \phi_{tl})_{N-1} \end{bmatrix}, \tag{1}$$

with $N$ being the number of slices (samples) along the aortic centerline.

### 3.4. Statistical shape model

The lengths of the aortic centerlines vary across patients, and are usually between 431 and 709 slices when sampled at 1 mm intervals. To establish correspondences between different patients, we align each dataset along the aortic centerline using iterative closest points (ICP). We then supersample each representation $\mathbf{D}_i$ to $N = 1000$ slices using linear interpolation.

To generate synthetic surface meshes of aortic dissections, SSM and ML approaches seem viable. ML usually performs best with a large and diverse database for initial training. Our database currently consists of 100 datasets, which is rather a small amount of data compared to previous work focusing on ML (Table 1). For this reason, and to systematically investigate the generation of synthetic dissections, we start with the construction of an SSM. This can later serve as a basis for comparison with ML approaches. Additionally, the SSM can be used as a means of data augmentation to supply ML approaches with a sufficient amount of data.

To compute an SSM, we perform a PCA on 80 of our total 100 datasets. Individual datasets $\mathbf{D}_i$ are reshaped into one-dimensional row vectors and stacked in a single $80 \times N$ matrix $\mathbf{M}$ as follows:

$$\mathbf{M} = \begin{bmatrix} \mathbf{D}_0 \\ \vdots \\ \mathbf{D}_{79} \end{bmatrix}. \tag{2}$$

To center the data, we subtract the mean shape $S_{mean}$ of the input data from the input data representations. Subsequently, we perform an SVD on the matrix $\mathbf{M}$, leading to the principal components (eigenvectors) $\Lambda$ and their corresponding eigenvalues $\lambda$. The eigenvectors are then sorted according to their variance.

A synthetic shape $S$ can be generated by multiplying the principal components $\Lambda$ with weights $\omega$ that are randomly sampled in the interval $[-\lambda, \lambda]$, and adding them to the mean shape $S_{mean}$ as follows

$$S = [\omega_0, \dots, \omega_i] \begin{bmatrix} \Lambda_0 \\ \vdots \\ \Lambda_i \end{bmatrix} + S_{mean}, \tag{3}$$

with $i$ being the number of chosen eigenvectors and weights.

### 3.5. Quality criteria

The chosen weight range provides a high shape variability between the generated aortic dissection datasets. However, synthetic shapes may contain physiological errors, i.e., they do not reflect correct anatomy, and must therefore either be corrected or, in severe cases, discarded. To filter unphysiological shapes, we use data-driven criteria evaluating the generated datasets based on their statistical properties. Additionally, we employ clinically-driven criteria, such as the start of the false lumen and the twisting of the true lumen.

**Data-Driven Criteria:** The first step consists of filtering all shapes that are not in the ranges of our input datasets. The evaluated properties are shown in Table 2. The measurements for our datasets lie in the ranges reported in other publications discussing the aorta and aortic dissection [25–28]. We also check whether the aorta or the true lumen shows abnormal changes in size (ellipse area) along the centerline. If the maximum and average amount of change are not in the limits of the input data, the generated shape is discarded.

**Clinically-Driven Criteria:** The twisting of the true lumen can affect the hemodynamics of the aorta, which in turn influences disease progression [29–31]. To avoid shapes with excessive twisting of the aorta and true lumen, generated datasets whose ellipse angles change beyond the limits of the input datasets are discarded. Shapes with true lumen ellipses larger than their corresponding (i.e., at the same centerline point) aortic ellipses are also discarded.

Additionally, we check the start of the false lumen along the aorta. To improve the robustness of the calculation, we define the beginning of the false lumen as the slice in MPR space where the false lumen exceeds 10% cross-sectional area of the aorta. The false lumen starts calculated based on the elliptical cross-sections deviate by less than

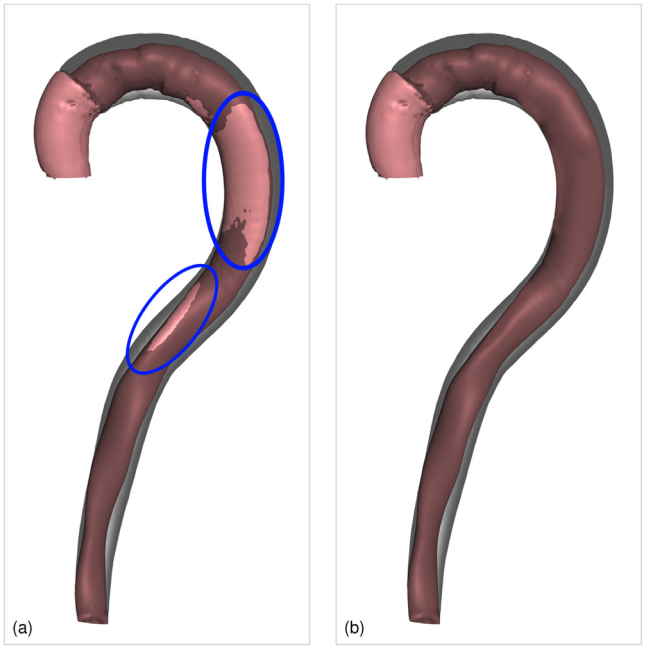


**Fig. 2.** Minor protrusions of the true lumen (blue circles) in the generated surface meshes (a) are corrected in (b) using boolean mesh operations truncating the true lumen mesh. This truncation step is faithful to real aortic dissection physiology in which the true lumen shares a large part of its wall with the aorta.

5% from the starts calculated based on the input segmentation and can therefore be used as a quality criterion to evaluate generated shapes.

These quality criteria can be used to generate aortic dissection datasets with specific physiological characteristics, such as a longer aorta, a shorter false lumen, and/or a thicker or thinner true lumen. However, the generation time increases as the number of predefined characteristics increases, as many generated shapes are discarded.

### 3.6. Surface mesh generation

Once a shape is accepted by our quality criteria, the aorta and true lumen surface meshes are generated based on their respective centerline-based representations. This is done by evenly sampling points on the circumference of each elliptical cross-section, followed by Poisson surface reconstruction [32]. However, consecutive ellipses might overlap in regions of high curvature, like the aortic arch. Poisson surface reconstruction mostly handles such cases well and produces watertight meshes. In some extreme cases, non-watertight meshes might be produced. Therefore, we automatically check each mesh for holes. Since we only encounter holes in less than 5% of all generated surface meshes a non-watertight surface mesh is discarded and a new mesh is generated. This means going back to step 5 in the workflow (Fig. 1) to generate a new synthetic shape and perform Poisson surface reconstruction.

### 3.7. Protrusion correction

Though our quality criteria filter most of the unphysiological shapes, some shapes contain true lumen ellipses that protrude through the aortic wall (Fig. 2). Since the true lumen usually shares a large portion of its wall with the aorta, these shapes do not have to be discarded and can be physiologically corrected. This is achieved by a boolean mesh operation that intersects the true lumen surface mesh with the aorta surface mesh, removing the protruding parts of the true lumen. The result is then a true lumen surface that is completely inside the aortic surface.

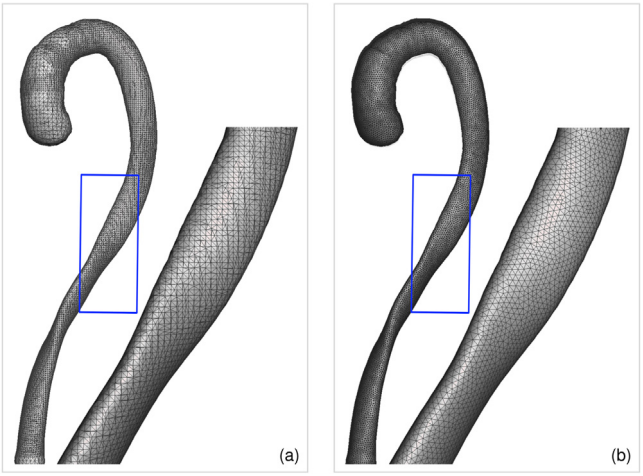


**Fig. 3.** After generating the surface meshes (a), they are remeshed to create mostly equilateral triangles with angles greater than 45° (b).

### 3.8. Remeshing

In the last automated step of our workflow (Fig. 1), the aorta and true lumen surface meshes are remeshed to create mostly equilateral triangles with angles greater than 45° (Fig. 3). This not only improves the quality of the surface meshes, but also prepares them for subsequent CFD simulations.

### 3.9. Computational fluid dynamics simulations

To perform CFD simulations, we require a single surface mesh encompassing the true and false lumen separated by a dissection flap and connected by the entry tear. To achieve this, we first extrude the true lumen surface mesh along the normal direction. This extruded true lumen mesh is then subtracted (using a boolean surface operation) from the aorta mesh to extract the false lumen surface mesh. The resulting false lumen and the original, non-extruded true lumen mesh are thus separated by the extrusion distance from the first step, generating a dissection flap between true and false lumen with uniform distance. We then remesh the false lumen surface. The results of the boolean mesh operations performed in this section can be seen in Fig. 4.

The true and false lumen meshes are then manipulated by manually adding an entry tear to connect both of them into a single surface mesh. The tear is generated by cutting a hole in the true lumen and false lumen mesh and connecting both. The inlets and outlets of the aorta are also specified manually. Then, the surface mesh is checked for any defects or low-quality areas and corrected if necessary.

We generate face information to differentiate between the inlet cross-section, the outlet of true and false lumen, and the vessel surface. The volumetric mesh is then generated. Finally, simulation input files to specify material parameters such as fluid density, viscosity and boundary conditions as well as parameters for numerical discretization are defined similarly to previous work [29]. The simulations are then run with a steady inlet velocity for 1000 timesteps.

### 3.10. Implementation

Our workflow is implemented in Python 3.10 using Scikit [33] for the SVD, Numpy [34] for interpolation and matrix processing, and MeshLab's [35] Python integration to generate the surface meshes. Autodesk Meshmixer [36] is used for boolean mesh operations and remeshing.

Remeshing is performed using the *target edge length* remesh mode with an edge length of 1 mm, and a regularity setting of 100. Iterations

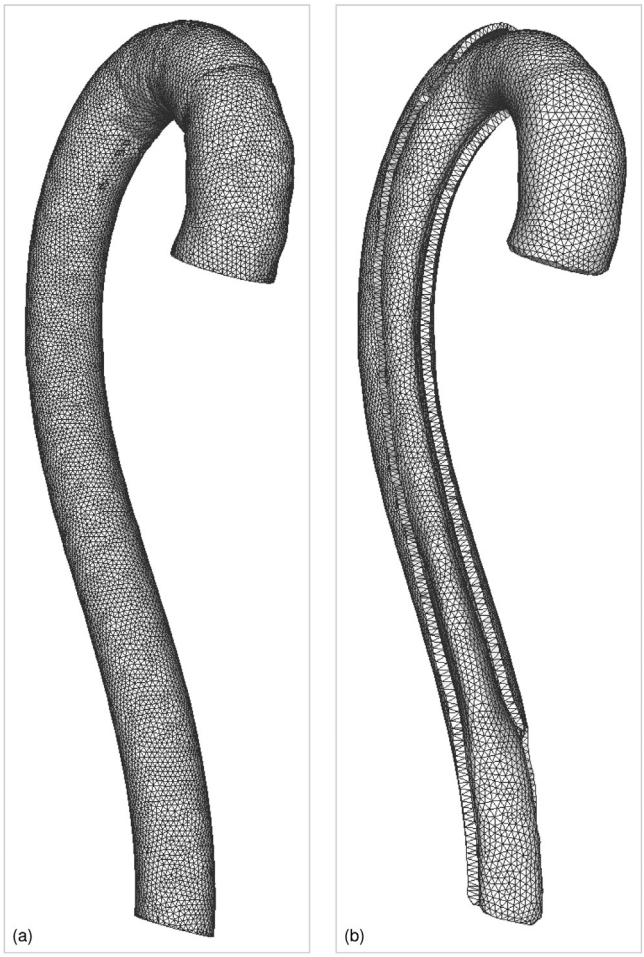


**Fig. 4.** Results of the applied boolean mesh operations to the aorta and true lumen mesh (a). The false lumen mesh is obtained by intersecting the aorta mesh with the true lumen mesh. Combining the true lumen and false lumen mesh results in (b) which is the CFD ready mesh used for our simulations.

are set to 25, transition to 0 mm, and smooth group boundaries is set to true. The sharp threshold is set to 12 and the *refined boundary* mode is used. CFD simulations are performed using SimVascular [37], executed on a high-performance computing system.

All calculations were performed on Windows 10 with an Intel i5-10600K with 32 GB RAM and an Nvidia GTX 3060 Ti. Preparation of 100 datasets and consecutive calculation of the SSM took approximately 10 minutes. Generating a single synthetic surface mesh and filtering for the quality criteria of the input cohort takes a few seconds ($<10$ s). Therefore, generating a cohort of 1000 datasets would take about 3 h.

## 4. Results and discussion

In this section, we investigate the effects of the different PCs on the centerline, the ellipse diameters and angles. We determine the most suitable number of PCs for the generation of synthetic shapes. Next, we measure the quality of the generated shapes by examining the true lumen twisting as a disease-specific quality criterion. Finally, we perform a qualitative assessment and run CFD simulations on a synthetic surface mesh.

### 4.1. Datasets

Our patient cohort consists of 100 datasets of Stanford type B aortic dissections obtained from CTA scans. These datasets cover 25 patients with initial and follow-up scans. Since aortic dissections vary physiologically from patient to patient, we use k-fold cross-validation and perform five iterations of PCA. The entire database was split using a train:test split of 4:1, resulting in 80 training datasets and 20 test datasets per iteration. In each iteration, we generate a synthetic cohort of 20 datasets.

### 4.2. Principal component analysis

Fig. 5 shows the cumulative variance across the PCs. In each iteration, we perform three different PCAs to compare the contribution of the true lumen and aorta towards the variance of the PCA. One is performed using only the ellipses and centerlines for the aorta, one using the true lumen ellipses and centerlines, and one combining the aorta and the true lumen. Our results are generated using the PCs of the combined. As the results of all iterations are similar, the numbers and values we present show the average across all iterations. Figures showing the results of each iteration can be found in the supplementary material.

Surprisingly, the aorta requires more PCs to encode its shape variability than the true lumen. One possible reason for this could be the higher longitudinal angle deviation of the aorta, which makes encoding more difficult. This increased deviation could be caused by an almost circular aorta in many places, which leads to rotating major and minor ellipse axes. Since the true lumen shape is less likely to be circular, its longitudinal twisting is more continuous (Section 4.4).

On average across all iterations, 90% of aortic shape variability are encoded at 22 PCs. The true lumen encodes 90% of shape variability at 17 PCs. Combining both, 90% of shape variability is reached at 28 PCs. The synthetic datasets used in the consecutive evaluation steps are generated using 28 PCs and filtered using the quality criteria presented in Section 3.5.

### 4.3. Aortic dissection representation

To evaluate the proposed representation, we test how much of the entire aorta volume is occupied by the true and false lumen. We calculate the lumen area ratios for each centerline point of our input data comparing the calculation results of the segmentation mask to the ellipse representation. Ellipses can capture the area of the true lumen and aorta with an average error of 5%. This indicates good suitability to approximate the aorta and the true lumen using ellipses.

To evaluate our generated synthetic datasets, we compared their ellipse area ratios with the input volume data. The percent of aortic area consumed by the true lumen is an important measure to indicate how much the true lumen is being compressed by the false lumen pressure. Unphysiological ratios between the true lumen and false lumen areas would be a good indication as to how well the SSM can capture this phenomenon. The area ratios along the centerline show a similar development compared to volume and ellipse ratios of the input data indicating that our generated datasets can properly capture the relationship between the true lumen and aorta area (Fig. 6).

### 4.4. True lumen twist

Aortic dissection can propagate through the aortic wall following a spiral trajectory. This spiral pattern influences aortic hemodynamics and affects disease progression. Understanding this pattern can improve computational models, enhancing the accuracy of CFD simulations and enabling better prediction of complications. Analyzing the torsion or twisting of vascular structure is important, e.g., when suturing vessels together, as discussed by Mistelbauer et al. [38]. To further evaluate how accurately the generated shapes represent actual aortic dissections, we examine the angular change of the major axis from the true lumen and aortic ellipses along the centerline. The major axis angle can differ within 20° between generated shapes. The average change in angles of

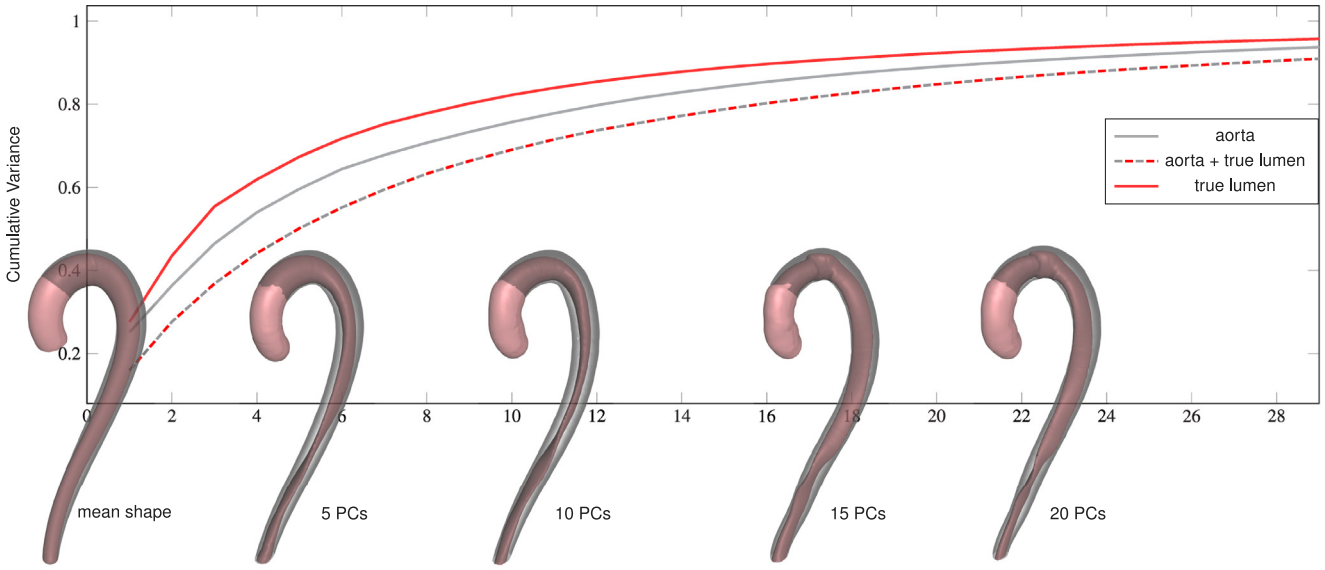


**Fig. 5.** Comparison of the cumulative variance across different PCAs. We performed three different PCAs to compare the influence the aorta and the true lumen have. The true lumen is easier to encode than the aorta, which has its variance distributed across a larger amount of principal components. On the x-Axis, the increase in shape variability is shown on a single generated dataset. Starting from the mean shape 5 PCs encode the general aortic and true lumen shape. From 10 to 20 PCs the aortic and true lumen shapes get more details such as an increase in the diameter of the true lumen in the aortic arch and the true lumen twist changes in the descending aorta.

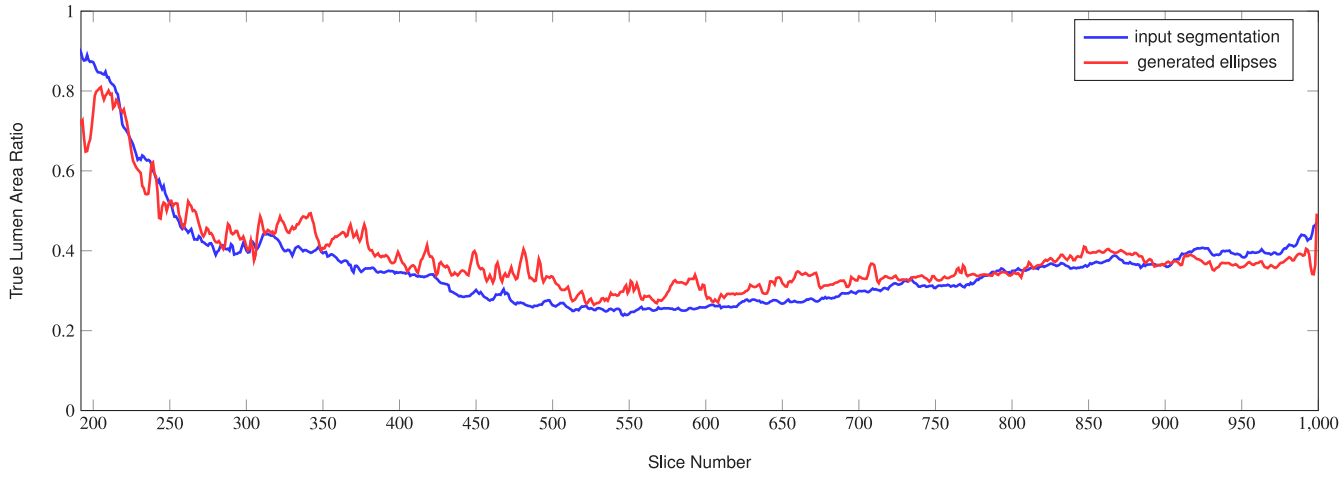


**Fig. 6.** Comparison of aorta area occupied by the true lumen across the input data and the generated datasets starting from the average false lumen start (centerline point 192). Before the false lumen starts the true lumen and aorta ratios are equal. The approximation of the aorta and true lumen using ellipses is accurate to 5% compared to the input volume data. Additionally, the generated datasets can properly capture the relationship between the true lumen and aorta area.

consecutive ellipses along the centerline is below 0.5°. These values are in line with our input data and indicate that we achieve good coverage of the shape space. Simultaneously, excessive twisting of the true lumen is avoided as well as sudden changes in angle which would result in unphysiological shapes. The true lumen twists a bit more than the aorta, with an average of 0.6°. The maximum angular change between consecutive ellipses is 10° for the aorta and 18° for the true lumen. This again shows that unphysiological twisting of both the aorta and the true lumen is avoided. Since the angular changes of the generated datasets are similar to those of the input data, across all PCA iterations, we cover the shape space well and faithfully capture the twisting of the true lumen and aorta.

### 4.5. Qualitative assessment

To ensure that the generated datasets are plausible from a clinical perspective, we consulted two radiologists with experience in aortic dissections (both co-authors). We randomly selected several datasets from the synthetic cohort we created and asked them to tell us whether these datasets looked authentic or what problems they showed. They concluded that the shape of the aorta appeared normal with the true lumen showing a realistic twisting and bending along the aorta. This indicates that the occurring spirality of the true lumen was properly captured by the SSM. Furthermore, the occupied volume along the dissection by the true lumen and the false lumen are plausible. The reduced volume of the true lumen, caused by increased pressure in the false lumen, is also evident in the generated datasets. The experts also pointed out that the model could be further improved by including branching vessels and adding communications between the two lumina in the form of entry and exit tear as well as fenestrations.

Some of the datasets showed a true lumen at the aortic arch enclosed by the false lumen. Although this configuration can indeed occur, it is not widespread, as our data sets show. To mitigate this problem, we can refine the quality criteria to ensure that only a smaller percentage of the generated datasets have this characteristic. This would also lead to a better match with the clinical observations of the two radiologists.

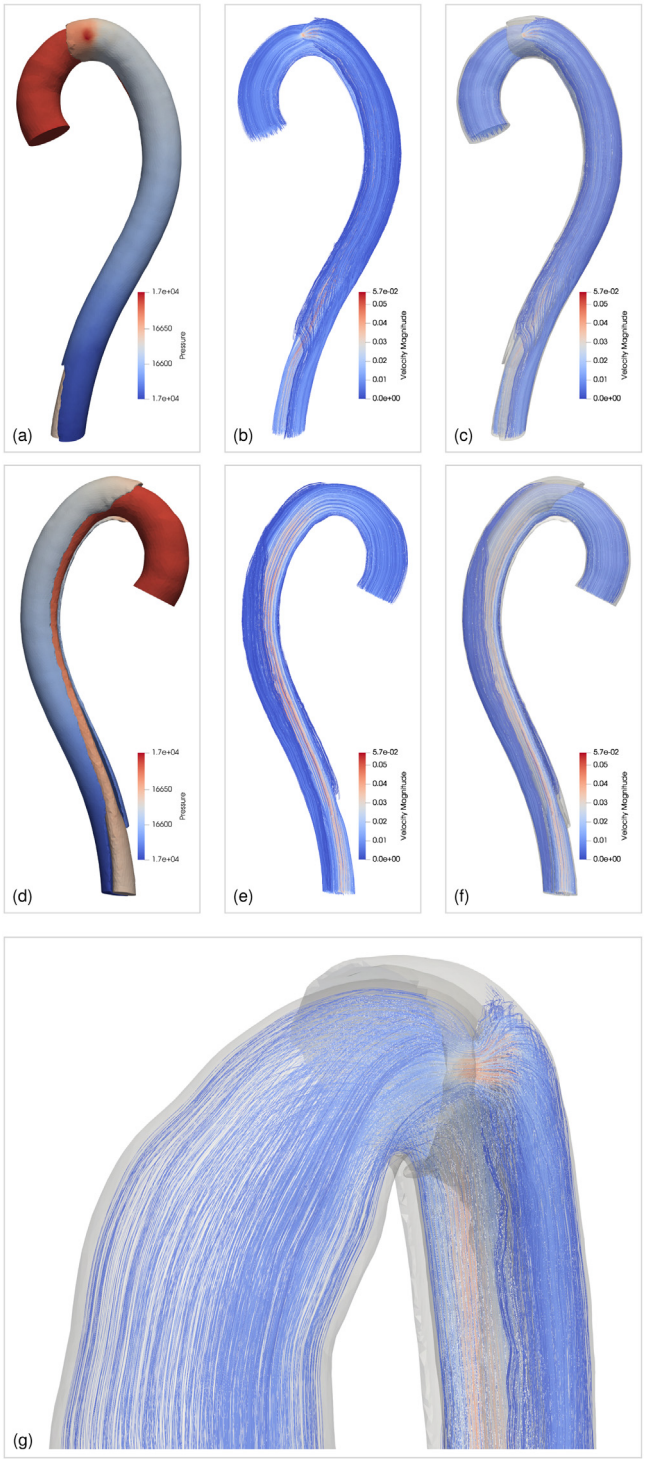


**Fig. 7.** Results of the CFD simulation performed on one randomly-selected synthetic surface mesh. Pressure is measured in Pa and velocity in m/s. (a, d) show pressure values mapped to the true lumen and false lumen walls, with low pressure in blue and high pressure in red. (b, e) show streamlines with velocity encoding, with low velocity in blue and high velocity in red. (e, f) show a combination of wall pressure and streamlines. Both the pressure and the velocity appear to be plausible. (g) shows a closeup of an impingement zone, caused by a flow jet, which can be seen on the aortic wall opposite the entry tear.

### 4.6. Computational fluid dynamics simulations

As a proof-of-concept and to demonstrate that the generated surface meshes can be used as a basis for CFD simulations, we performed such a simulation with one surface mesh. We assumed a Newtonian fluid with a viscosity of 0.004 kg/ms and a steady inflow with a flow rate of 4.3 L/min. At the fluid outlets of the true lumen and false lumen, we prescribed a resistance boundary condition and tuned the resistance parameters such that an approximate pressure of 125 mmHg (or 16665.3 Pa) was obtained in the aorta (Fig. 7d). The outer wall of the aorta was modeled as rigid. The volumetric mesh was generated with Tetgen [39] and simulations were performed with the finite element solver svFSI [37]. More details on flow simulations of aortic dissection can be found in the work of Bäumler et al. [29].

Simulation results are shown in Fig. 7. With this proof-of-concept, we aimed to highlight one use case of synthetic aortic dissection surface meshes and show that the generated surface meshes are suitable for CFD applications with minimal postprocessing. Just as in patient-specific geometries derived from medical imaging data, we applied physiological material parameters as well as physiological boundary conditions, and achieved simulation results with realistic pressure and velocity values.

### 4.7. Limitations

Our input datasets only consist of volumetric data segmented into true and false lumen. They do not contain landmark information such as locations of branching vessels, entry and exit tears, or fenestrations. Therefore, our generated datasets can only model the true and false lumen inside the aorta. Only the location of the entry tears can be approximated using the false lumen starts (Section 3.5).

## 5. Conclusion and future work

We proposed a method to model synthetic aortic dissection surface meshes using statistical shape modeling combined with the automatic rejection of unphysiological shapes using clinically- and data-driven quality criteria. Furthermore, we presented the processing of the generated surface meshes to truncate the true lumen and prepare the surface meshes for CFD simulations. The generated datasets were deemed plausible from a clinical perspective and CFD simulations were performed as proof-of-concept to confirm the suitability of our generated surface meshes.

In the future, we would like to include landmark information but as of now, we do not have a sufficient amount of datasets that contain complete segmentations of true and false lumen as well as landmark locations. The elliptical cross-sectional models of the aorta and the true lumen could be improved to more closely approximate their shapes. Elliptic Fourier descriptors could be a suitable alternative [22]. Since we only model the false lumen indirectly, the simultaneous modeling of the true and false lumen with ellipses leads to many overlaps that cannot be easily resolved. This could be avoided by modeling only the aortic wall and the dissection flap.

The generation of synthetic aortic dissection surface meshes using machine learning is another promising future avenue. This aligns with our long-term goal of creating a comprehensive model that can generate customized datasets of aortic dissections from disease-specific input criteria, such as the type of dissection, the number of fenestrations, and the supplying lumen of branch vessels. To achieve this, a large amount of data is required, which can be generated by our presented workflow.

## CRediT authorship contribution statement

**Kai Ostendorf:** Writing – original draft. **Kathrin Bäumler:** Data curation. **Domenico Mastrodicasa:** Writing – review & editing. **Dominik Fleischmann:** Supervision. **Bernhard Preim:** Supervision. **Gabriel Mistelbauer:** Supervision.

## Declaration of competing interest

The authors declare the following financial interests/personal relationships which may be considered as potential competing interests: Otto-von-Guericke University Magdeburg, Germany Stanford University School of Medicine, USA

## Data availability

The data that has been used is confidential.

## Acknowledgments

The medical data sets were acquired at Stanford School of Medicine, approved by the institutional review board (IRB#41660). Open access funding enabled and organized by Projekt DEAL.

## Appendix A. Supplementary data

Supplementary material related to this article can be found online at https://doi.org/10.1016/j.cag.2024.104070.

## References

[1] Wundram M, Falk V, Eulert-Grehn JJ, Herbst H, Thurau J, Leidel BA, et al. Incidence of acute type A aortic dissection in emergency departments. Sci Rep 2020;10(7434). http://dx.doi.org/10.1038/s41598-020-64299-4.

[2] Danu M, Nita CI, Vizitiu A, Suciu C, Itu LM. Deep learning based generation of synthetic blood vessel surfaces. In: Proceedings of the international conference on system theory, control and computing. IEEE; 2019, p. 662–7. http://dx.doi.org/10.1109/icstcc.2019.8885576.

[3] Feldman P, Fainstein M, Siless V, Delrieux C, Iarussi E. VesselVAE: Recursive variational autoencoders for 3D blood vessel synthesis. 2023, http://dx.doi.org/10.48550/ARXIV.2307.03592, arXiv.

[4] Thamsen B, Yevtushenko P, Gundelwein L, Lamecker H, Kühne T, Goubergrits L. Unsupervised learning and statistical shape modeling of the morphometry and hemodynamics of coarctation of the aorta. In: Medical image computing and computer assisted intervention. Springer; 2020, p. 776–85. http://dx.doi.org/10.1007/978-3-030-59719-1_75.

[5] Wiputra H, Matsumoto S, Wagenseil JE, Braverman AC, Voeller RK, Barocas VH. Statistical shape representation of the thoracic aorta: Accounting for major branches of the aortic arch. Comput Methods Biomech Biomed Eng 2022;1–15. http://dx.doi.org/10.1080/10255842.2022.2128672.

[6] Catalano C, Agnese V, Gentile G, Raffa GM, Pilato M, Pasta S. Atlas-based evaluation of hemodynamic in ascending thoracic aortic aneurysms. Appl Sci 2021;12(1):394. http://dx.doi.org/10.3390/app12010394.

[7] Thamsen B, Yevtushenko P, Gundelwein L, Setio AAA, Lamecker H, Kelm M, et al. Synthetic database of aortic morphometry and hemodynamics: Overcoming medical imaging data availability. IEEE Trans Med Imaging 2021;40(5):1438–49. http://dx.doi.org/10.1109/tmi.2021.3057496.

[8] Daily PO, Trueblood HW, Stinson EB, Wuerflein RD, E.Shumway N. Management of acute aortic dissections. Ann. Thorac. Surg. 1970;10(3):237–47. http://dx.doi.org/10.1016/s0003-4975(10)65594-4.

[9] Romero P, Lozano M, Martínez-Gil F, Serra D, R. Sebastián, Lamata P, et al. Clinically-driven virtual patient cohorts generation: An application to aorta. Front Physiol 2021;12:713118. http://dx.doi.org/10.3389/fphys.2021.713118.

[10] Beetz M, Banerjee A, Grau V. Multi-domain variational autoencoders for combined modeling of MRI-based biventricular anatomy and ECG-based cardiac electrophysiology. Front Physiol 2022;13. http://dx.doi.org/10.3389/fphys.2022.886723.

[11] Cootes TF, Taylor CJ. Active shape models — 'smart snakes'. In: Proceedings of the british machine vision conference. London: Springer; 1992, p. 266–75. http://dx.doi.org/10.1007/978-1-4471-3201-1_28.

[12] Heimann T, Meinzer HP. Statistical shape models for 3D medical image segmentation: A review. Med. Image Anal. 2009;13(4):543–63. http://dx.doi.org/10.1016/j.media.2009.05.004.

[13] Bridio S, Luraghi G, Ramella A, Rodriguez Matas JF, Dubini G, Luisi CA, et al. Generation of a virtual cohort of patients for in silico trials of acute ischemic stroke treatments. Appl Sci 2023;13(18):10074. http://dx.doi.org/10.3390/app131810074.

[14] Verstraeten S, Hoeijmakers M, Tonino P, Brüning J, Capelli C, van de Vosse F, et al. Generation of synthetic aortic valve stenosis geometries for in silico trials. Int J Numer Methods Biomed Eng 2023;40(1). http://dx.doi.org/10.1002/cnm.3778.

[15] Romero P, Santos S, Sebastian R, Martinez-Gil F, Serra D, Calvillo P, et al. Reconstruction of the aorta geometry using canal surfaces. In: Proceedings of the international conference on computational and mathematical biomedical engineering. 2019.

[16] Durrleman S, Prastawa M, Charon N, Korenberg JR, Joshi S, Gerig G, et al. Morphometry of anatomical shape complexes with dense deformations and sparse parameters. NeuroImage 2014;101:35–49. http://dx.doi.org/10.1016/j.neuroimage.2014.06.043.

[17] Petersen SE, Matthews PM, Bamberg F, Bluemke DA, Francis JM, Friedrich MG, et al. Imaging in population science: Cardiovascular magnetic resonance in 100,000 participants of UK biobank - rationale, challenges and approaches. J. Cardiovasc. Magn. Reson. 2013;15(46). http://dx.doi.org/10.1186/1532-429x-15-46.

[18] Felkel P, Wegenkittl R, Buhler K. Surface models of tube trees. In: Proceedings computer graphics international. IEEE; 2004, p. 70–7. http://dx.doi.org/10.1109/cgi.2004.1309194.

[19] Catmull E, Clark J. Recursively generated B-spline surfaces on arbitrary topological meshes. Comput Aided Des 1978;10(6):350–5. http://dx.doi.org/10.1016/0010-4485(78)90110-0.

[20] Wang W, Jüttler B, Zheng D, Liu Y. Computation of rotation minimizing frames. ACM Trans Graph 2008;27(1):1–18. http://dx.doi.org/10.1145/1330511.1330513.

[21] Mistelbauer G, Morar A, Varchola A, Schernthaner R, Baclija I, Köchl A, et al. Vessel visualization using curvicircular feature aggregation. Comput Graph Forum 2013;32(3):231–40. http://dx.doi.org/10.1111/cgf.12110.

[22] Mistelbauer G, Rössl C, Bäumler K, Preim B, Fleischmann D. Implicit modeling of patient-specific aortic dissections with elliptic Fourier descriptors. Comput Graph Forum 2021;40(3):423–34. http://dx.doi.org/10.1111/cgf.14318.

[23] Meister F, Houle H, Nita C, Puiu A, Itu LM, Rapaka S. Artificial intelligence for computational modeling of the heart. Academic Press; 2019, p. 190–203, (Chapter 6.2 - Aortic coarctation).

[24] Kretschmer J, Godenschwager C, Preim B, Stamminger M. Interactive patient-specific vascular modeling with sweep surfaces. IEEE Trans Vis Comput Graphics 2013;19(12):2828–37. http://dx.doi.org/10.1109/tvcg.2013.169.

[25] Dotter CT, Roberts DJ, Steinberg I. Aortic length: Angiocardiographic measurements. Circulation 1950;2(6):915–20. http://dx.doi.org/10.1161/01.cir.2.6.915.

[26] Nienaber CA, Clough RE, Sakalihasan N, Suzuki T, Gibbs R, Mussa F, et al. Aortic dissection. Nat. Rev. Dis. Prim. 2016;2(1). http://dx.doi.org/10.1038/nrdp.2016.53.

[27] Gameraddin M. Normal abdominal aorta diameter on abdominal sonography in healthy asymptomatic adults: impact of age and gender. J Radiat Res Appl Sci 2019;12(1):186–91. http://dx.doi.org/10.1080/16878507.2019.1617553.

[28] Heuts S, Adriaans BP, Rylski B, Mihl C, Bekkers SCAM, Olsthoorn JR, et al. Evaluating the diagnostic accuracy of maximal aortic diameter, length and volume for prediction of aortic dissection. Heart 2020;106(12):892–7. http://dx.doi.org/10.1136/heartjnl-2019-316251.

[29] Bäumler K, Vedula V, Sailer AM, Seo J, Chiu P, Mistelbauer G, et al. Fluid–structure interaction simulations of patient-specific aortic dissection. Biomech Model Mechanobiol 2020;19(5):1607–28. http://dx.doi.org/10.1007/s10237-020-01294-8.

[30] Takahashi K, Sekine T, Miyagi Y, Shirai S, Otsuka T, Kumita S, et al. Four-dimensional flow analysis reveals mechanism and impact of turbulent flow in the dissected aorta. Eur J Cardiothorac Surg 2021;60(5):1064–72. http://dx.doi.org/10.1093/ejcts/ezab201.

[31] Ruiz-Muñoz A, Guala A, Dux-Santoy L, Teixidó-Turà G, Servato ML, Valente F, et al. False lumen rotational flow and aortic stiffness are associated with aortic growth rate in patients with chronic aortic dissection of the descending aorta: a 4d flow cardiovascular magnetic resonance study. J. Cardiovasc. Magn. Reson. 2022;24(1):20. http://dx.doi.org/10.1186/s12968-022-00852-6.

[32] Kazhdan M, Hoppe H. Screened Poisson surface reconstruction. ACM Trans Graph 2013;32(3):1–13. http://dx.doi.org/10.1145/2487228.2487237.

[33] Pedregosa F, Varoquaux G, Gramfort A, Michel V, Thirion B, Grisel O, et al. Scikit-learn: Machine learning in python. J Mach Learn Res 2011;12(85):2825–30, URL: http://jmlr.org/papers/v12/pedregosa11a.html.

[34] Harris CR, Millman KJ, van der Walt SJ, Gommers R, Virtanen P, Cournapeau D, et al. Array programming with numpy. Nature 2020;585(7825):357–62. http://dx.doi.org/10.1038/s41586-020-2649-2.

[35] Cignoni P, Callieri M, Corsini M, Dellepiane M, Ganovelli F, Ranzuglia G. Meshlab: an open-source mesh processing tool. 2008, http://dx.doi.org/10.2312/LOCALCHAPTEREVENTS/ITALCHAP/ITALIANCHAPCONF2008/129-136.

[36] Autodesk. Meshmixer. 2020, URL: https://meshmixer.com/.

[37] Updegrove A, Wilson NM, Merkow J, Lan H, Marsden AL, Shadden SC. SimVascular: An open source pipeline for cardiovascular simulation. Ann Biomed Eng 2016;45(3):525–41. http://dx.doi.org/10.1007/s10439-016-1762-8.

[38] Mistelbauer G, Zettwitz M, Schernthaner R, Fleischmann D, Teutsch C, Preim B. Visual assessment of vascular torsion using ellipse fitting. In: Eurographics workshop on visual computing for biology and medicine. 2018, http://dx.doi.org/10.2312/VCBM.20181238.

[39] Si H. TetGen, a delaunay-based quality tetrahedral mesh generator. ACM Trans Math Software 2015;41(2):1–36. http://dx.doi.org/10.1145/2629697.